

In-situ formed 3D hybrid framework of lithiophilic $\text{Li}_2\text{Cu}_3\text{Zn}$ modified Li_xCu alloy nanowires towards dendrite-free Li metal anode

Hang Liu^{a,b}, Chaohui Wei^b, Zhicui Song^{a,b}, Yujie Wu^{a,b}, Donghang Wang^b, Aijun Zhou^{a,b}, Jingze Li^{a,b*}

^a School of Materials and Energy, University of Electronic Science and Technology of China, Chengdu 611731, P. R. China

^b Huzhou Key Laboratory of Smart and Clean Energy, Yangtze Delta Region Institute (Huzhou), University of Electronic Science and Technology of China, Huzhou 313001, P. R. China

Corresponding author E-mail: lijingze@uestc.edu.cn (J. Z. Li)

Experimental section

Materials preparation

The melt-coating experiment was conducted in a glove box filled with argon gas. To fabricate the L40CZ0.4 alloy, Li (99.9%, Chengdu Denway Newtype Metal Material Co., Ltd.), Cu (99.9%, Shenzhen Wantong Meixin Technologies Co., Ltd.), and Zn (99.9%, Aladdin. Reagent Co., Ltd.) were weighed in an atomic ratio of 40:1:0.4, respectively. These metals were then placed into a crucible and subsequently positioned on a heating platform at 400 °C. The mixture was continuously stirred to obtain a molten slurry, resulting in the formation of the L40CZ0.4 alloy. Then the temperature of the heating platform was reduced to 320 °C, and the Cu foil was secured in place on the heating platform. Controlling the distance between the scraper and the Cu foil, the molten L40CZ0.4 alloy was poured onto the Cu foil, and the Cu foil was rotated at a rate of 6 r/min. After natural cooling, the L40CZ0.4@Cu anode was finally obtained.

Materials characterization

The phase identification was carried out in an X-ray diffractometer (XRD, Rigaku) using Cu K α wave ($\lambda = 0.154$ nm) at an acceleration voltage of 40.0 kV with a scanning speed of 10°/min. Encapsulating the Li-containing samples by polyimide tape to avoid the oxidation during testing. The morphology and elemental distribution of the samples were investigated by using scanning electron microscopy (SEM, Phenom) and energy-dispersive spectroscopy (EDS).

Electrochemical measurements

Symmetric and full cells were assembled in CR2032-type coin cells with a 2325 Celgard separator. The ether-based electrolyte was 1 M Li hexafluorophosphate (LiPF₆) in ethylene carbonate (EC) /diethyl carbonate (DEC) (v/v = 1:1) with 5 vol% fluoroethylene carbonate (FEC). The ether-based electrolyte was 1 M Li bis(tri-fluoromethanesulphonyl) imide (LiTFSI) in (1,3-dioxolane (DOL)/1,2-dimethoxyethane (DME) (v/v = 1:1) with 2 wt% LiNO₃. The areal loading of LFP was ~ 11.3 mg cm⁻². Galvanostatic charge/discharge performance was measured by NEWARE multichannel battery tester (Shenzhen, China). Electrochemical impedance spectroscopy (EIS, 100 kHz to 0.01 Hz) and the Tafel curves (1 mV s⁻¹, -0.2 to 0.2 V) of symmetric cells were tested on a CHI760D electrochemical workstation (Chenhua, Tianjin, China).

The ACE tests were conducted on Li||Cu cells assembled with three groups of samples using ether-based electrolytes. In ACE tests, the Li||Cu cells were initially subjected to a stripping/plating process with a total capacity of 3 mAh to form a well-established SEI, and then cycled 30 cycles at 1 mA cm⁻², 1 mAh cm⁻². Finally, all remaining Li on Cu foil was stripped at 1 mA cm⁻² until the voltage reached 1 V.

The ACE was calculated by the following formula (the first adjustment period is not

calculated): $C_{a,v} = \frac{nQ_C + Q_S}{nQ_C + Q_T}$, The number of cycles is denoted by n, the fixed charge used during cycling is Q_C, and the charge stripped from the Cu foil at the end is Q_S. The initial pre-deposited charge on the Cu foil is Q_T. The charge can be calculated using areal capacity as a substitute. Therefore, the cycle number is 30. The fixed areal capacity used during cycling is 1 mAh cm⁻², and the initial pre-deposited areal capacity on the Cu foil is 3 mAh cm⁻².

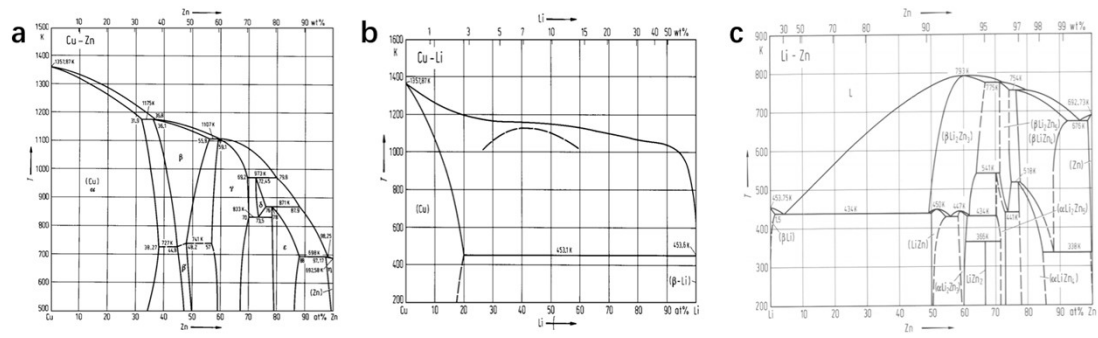


Fig. S1: The binary Alloy Phase Diagrams of (a) Cu-Zn, (b) Li-Cu, and (c) Li-Zn.¹

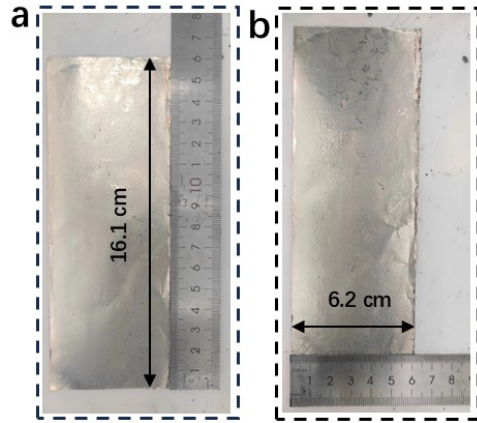


Fig. S2. The optical photos showing the width and thickness of LCZ@Cu film.

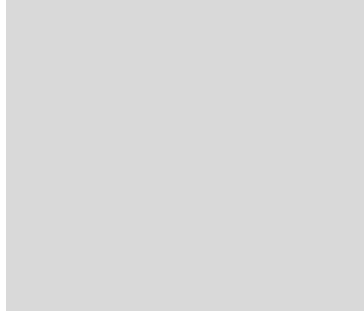


Fig. S3. The optical photos demonstrating the mechanical flexibility of LCZ@Cu film.

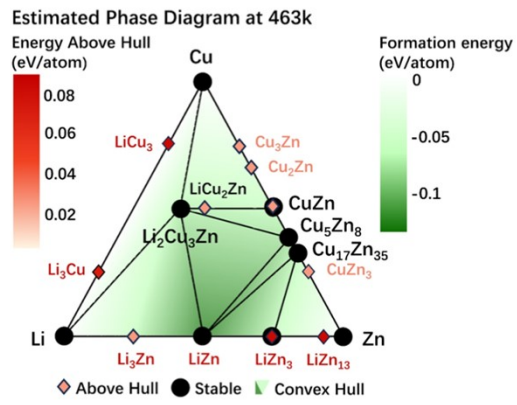


Fig. S4. The calculated ternary phase diagram of the Li-Cu-Zn alloy at 463 K.

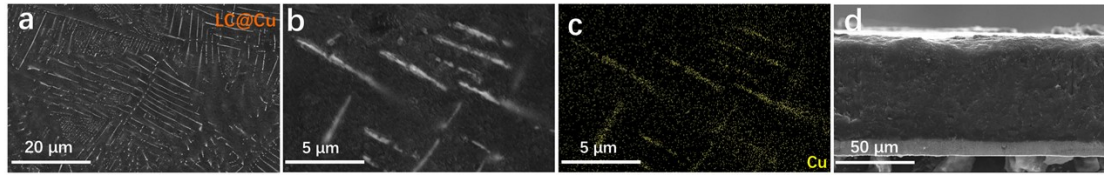


Fig. S5. (a, b) Top-view SEM images of the LC@Cu. (c) EDS mapping image of the (b). (d) Cross-sectional SEM image of LC@Cu.

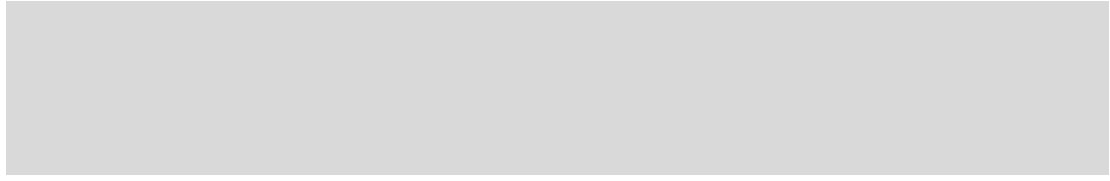


Fig. S6. (a, b) Top-view SEM images of the L@Cu. (c) EDS mapping image of the (b). (d) Cross-sectional SEM image of L@Cu.

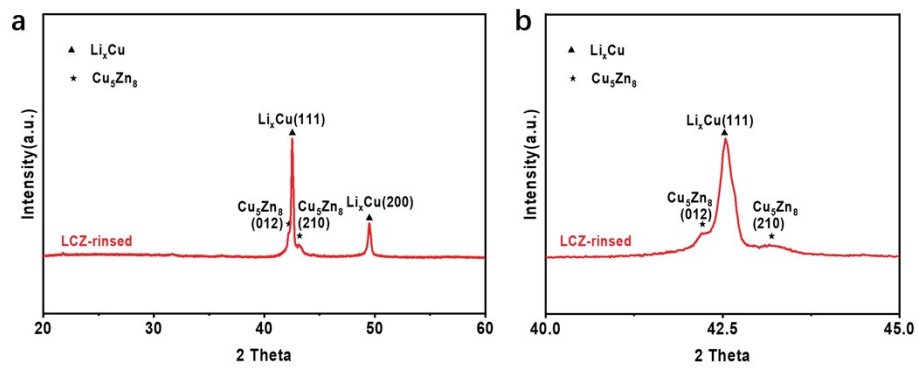


Fig. S7. (a) XRD pattern of the hybrid framework of LCZ sample without substrate after rinsing. (b) corresponding zoomed-in XRD pattern.

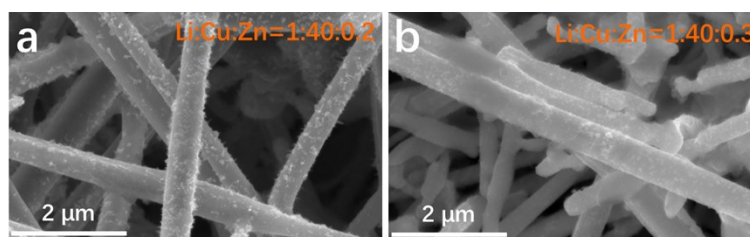


Fig. S8. Top-view SEM images of $\text{Li}_4\text{CuZn}_{0.2}@Cu$ (a) and $\text{Li}_4\text{CuZn}_{0.3}@Cu$ (b).

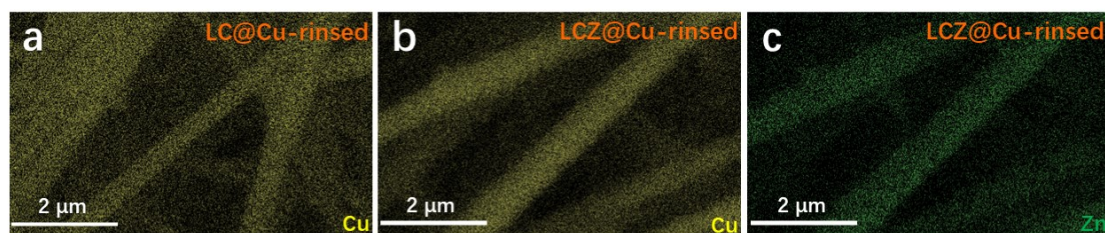


Fig. S9. The corresponding EDS mapping images of (a) the rinsed L@Cu and (b-c) the rinsed LCZ@Cu.

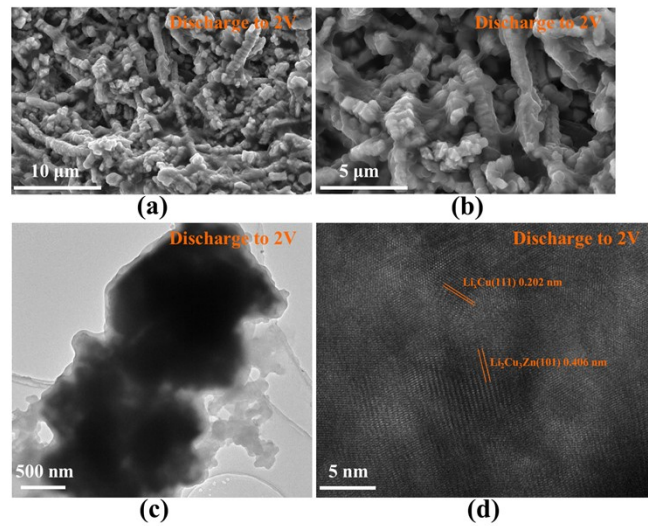


Fig. S10. (a, b) Top-view SEM and (c, d) TEM images of the LCZ after delithiation to 2 V.

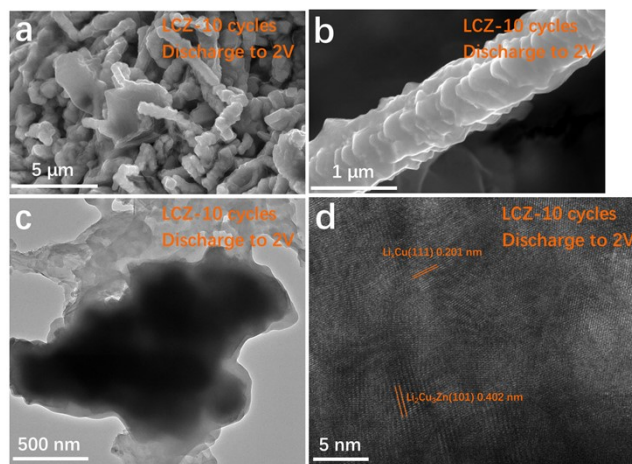


Fig. S11. (a, b) Top-view SEM and (c, d) TEM images of the LCZ after delithiation to 2 V in ether-based electrolyte after 10 cycles with 1 mA h cm^{-2} at 1 mA cm^{-2} .

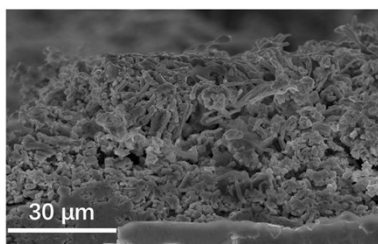


Fig. S12. Cross-sectional SEM image of the LCZ@Cu after delithiation to 1 V.

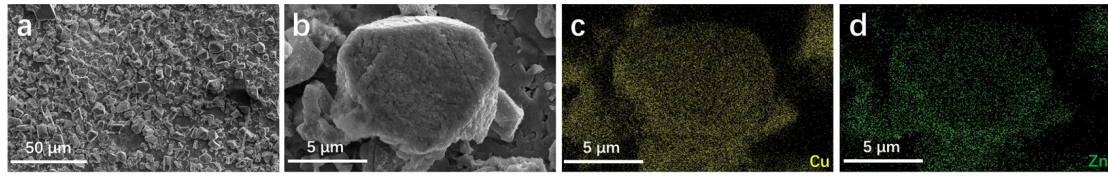


Fig. S13. (a, b) Top-view SEM images of the Cu foil surface of rinsed LCZ@Cu after scraping off the nanowire scaffold. (c, d) EDS mapping images of (b).

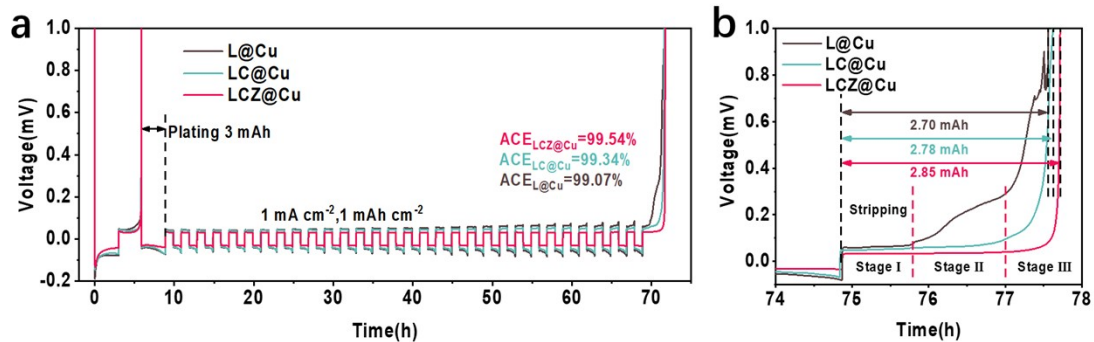


Fig. S14. (a) ACE for 30 cycles of Li stripping/plating at 1 mA cm⁻², 1 mAh cm⁻² in ether-based electrolyte. (b) The last delithiation process after 30 cycles in ACE measurement.

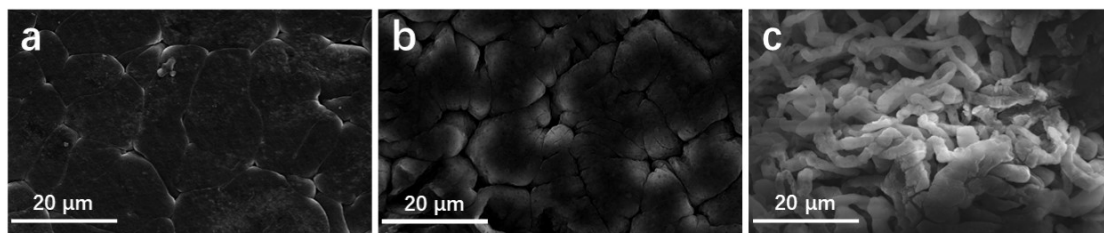


Fig. S15. Top-view SEM images of (a) LCZ@Cu, (b) LC@Cu, (c) L@Cu(c) after 100 cycles at 1 mA h cm⁻², 1 mA cm⁻².

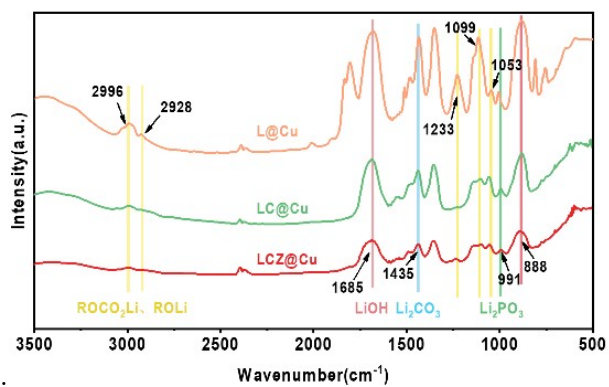


Fig. S16. FTIR spectra of LCZ@Cu, LC@Cu and L@Cu(c) after 50cycles in ester-based electrolyte at 1 mA cm^{-2} , 1 mAh cm^{-2} .

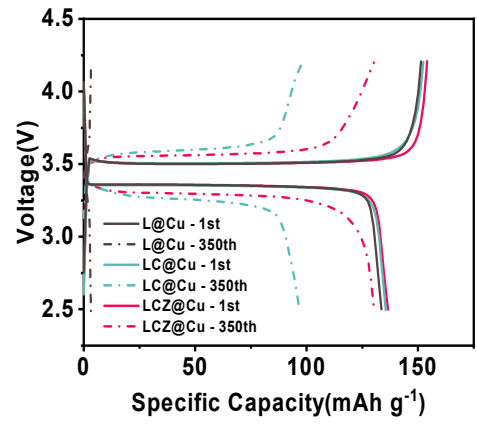


Fig. S17. The voltage-capacity curves of L@Cu, LC@Cu, and LCZ@Cu at the 1st and 350th cycle.

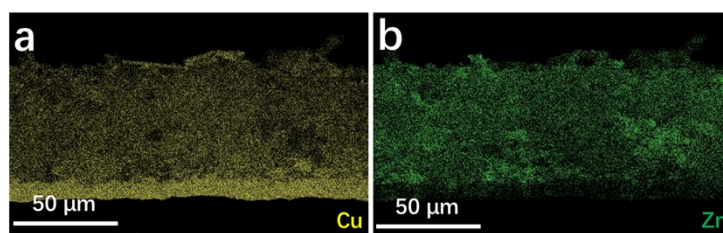


Fig. S18. The corresponding cross-sectional EDS mappings of the rinsed LCZ@Cu.

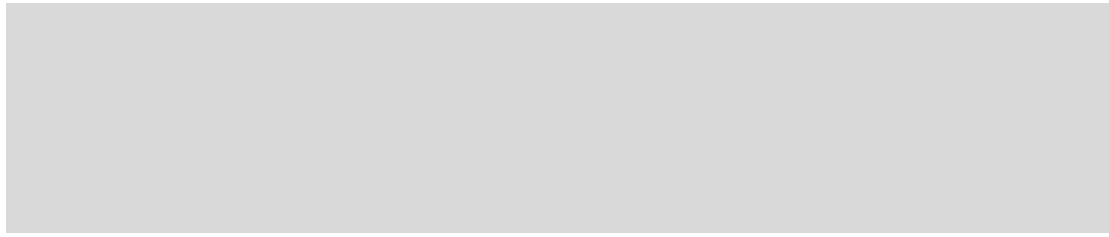


Fig. S19. (a) Cross-sectional SEM image and (b-c) the corresponding EDS mappings of the Cu foil substrate of the rinsed LCZ@Cu after scraping off the nanowire scaffold..

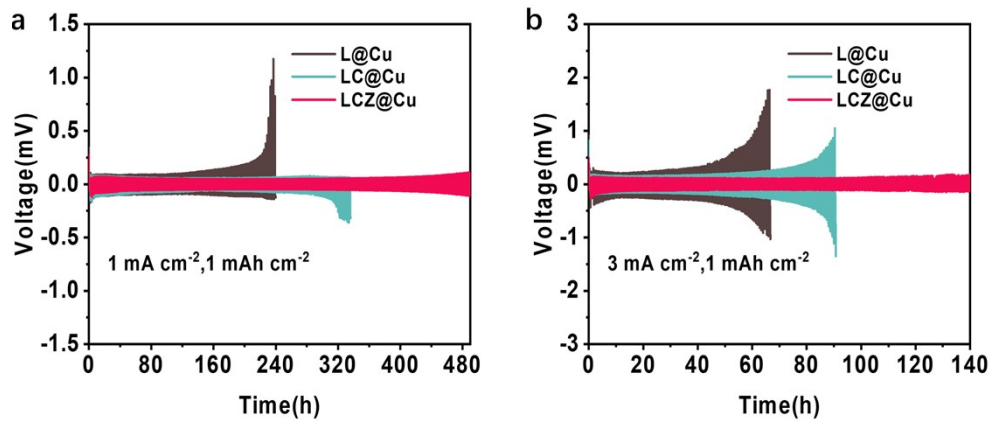


Fig. S20. The cells assembled with LCZ@Cu, LC@Cu, and L@Cu in ester-based electrolyte. The long-term cycling stabilities of symmetric cells under testing conditions (a) 1 mA cm^{-2} and 1 mAh cm^{-2} , (b) 3 mA cm^{-2} and 1 mAh cm^{-2} .

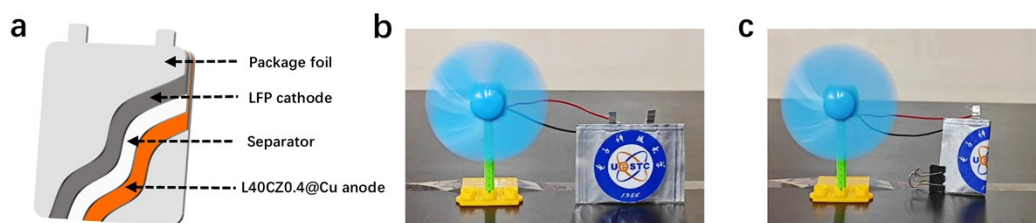


Fig. S21. (a) Schematic illustration of the as-assembled pouch cell. The pouch cell powers a small fan (b) before and (c) after 180° folding.

Table S1. Comparison of electrochemical performances of the symmetric cell in reported work and this work.

Electrode	Electrolyte type	Total capacity (mAh·cm ⁻²)	Current density (mA·cm ⁻²)	Cycle capacity (mAh·cm ⁻²)	Time (h)	Reference
Li/LiZn@Cu	1 M LiTFSI in DOL/DME (v/v = 1:1) with 1 wt% LiNO ₃	4.4	0.5	1	1200	Nature Communications, 2024, 15, 1354.
Cu@LC21	1 M LiTFSI in DME/DOL (v/v = 1:1) with 1 wt% LiNO ₃	6	1	1	540	Journal of Colloid and Interface Science, 2023, 630, 901-908
LLP	1 M LiTFSI in DME/DOL (v/v = 1:1) with 2 wt% LiNO ₃	4	1	1	500	Nano Research, 2024, 17, 4031-4038
Cu-Ge@Li	1 M LiTFSI in DME/DOL (v/v = 1:1) with 0.25 M LiNO ₃	5	0.5	1	1000	Small, 2023, 19.
Se@CC	1 M LiTFSI in DOL/DME (v/v = 1:1) with 2 wt% LiNO ₃	9.83	1	1	600	ACS Applied Materials & Interfaces, 2024, 16, 7327
10mg-Li@Pb@CC	1 M LiPF ₆ in EC/EMC (v/v = 3:7)	49.17	1	1	4648	Journal of Materials Chemistry A, 2022, 10, 8424-8431
LCZ@Cu	1 M LiTFSI in DOL/DME (v/v = 1:1) with 2 wt% LiNO₃	7.48	1	1	1400	This Work
	1 M LiPF₆ in EC/DEC (v/v = 1:1) with 5 vol% FEC	7.48	1	1	490	

Notes and references

1. H. Okamoto and T. Massalski, *ASM International, Materials Park, OH, USA*, 1990, **12**, 3528-3531.